Journal of Applied Geophysics 75 (2011) 151–160

Contents lists available at ScienceDirect

Journal of Applied Geophysics

journal homepage: www.elsevier.com/locate/jappgeo

# Applying GPR-amplitude wave maps and Am-scans as a semi-quantitative approach to the internal structure of sediments

Ó. Pueyo-Anchuela *, A.M. Casas-Sainz, A. Pocoví Juan, M.A. Soriano

*Departamento de Ciencias de la Tierra, Universidad de Zaragoza, Spain*

ARTICLE INFO

*Article history:*
Received 23 September 2009
Accepted 2 July 2011
Available online 3 September 2011

*Keywords:*
Ground penetrating radar
Unshielded device
Shielded device
Amplitude grid maps
Semiquantitative approach

ABSTRACT

In this work we analyse the applicability of amplitude grid maps to the routine of geological surveys by means of GPR (ground penetrating radar). Although amplitude grid maps have been commonly used in archaeological surveys, their use in geological prospecting (including the detection of voids and determination of the internal geometry of sedimentary bodies) is not widespread. The direct analysis of GPR-profiles permits the analysis of geometrical features and other qualitative aspects that can be related to changes in EM properties. Aspects such as changes in the density of the banded disposition in radargrams, loss of reflector definition or higher scattering in particular zones of the profiles can give useful, though non-quantitative, information. The GPR wave-amplitude is a qualitative measurement of magnetic properties that can be processed as a semi-quantitative layout. The main differences observed in changing wave amplitude are related to the surveyed materials and their geometry. These changes produce variations in the relative wave amplitude or vertical wave-phase changes related to differences in the propagation velocity, the attenuation factor, the reflectivity and the geometry of the materials. Maps based on the lateral correlation between profiles (C-scans) or the lateral correlation of wave amplitudes along the same profile (as a tomography or Am-scans) permit the analysis of these changes. Variations in amplitude grid maps or Am-scans are related to (i) geometrical changes of surveyed materials, (ii) changes in the dielectric constant, and (iii) changes in the potential penetration depth (higher attenuation in particular zones of a profile) than can be correlated to the type, state or clay content of subsoil materials. Direct analysis of exposures helps to constrain interpretation using the geometrical features in radargrams resulting from the geological structure. In the same way, analysis of geometrical features in radargrams, together with time-slices of C-scans, can be used to determine the areal distribution of changes in the subsoil and approach the changes in EM properties. An example with parallel profiles and different devices, constrained by means a broadband multifrequency EM survey is shown.



## 1. Introduction

Ground penetrating radar (GPR) is a qualitative geophysical technique related to the emission, propagation, diffraction, scattering and reflection of electromagnetic (EM) waves in the subsoil. The wide range of central frequencies of GPR devices provides a wide potential field of application. The usual devices with central frequencies between 25 MHz and 2.5 GHz offer penetration depths that range from a millimeter scale to tens of meters. In the same way, resolution in GPR devices provides ranges from millimeter to several meters (considering, for example, the horizontal discrimination resolution obtained from the first Fresnel zone) or one order of magnitude higher in the vertical, depending on the propagation velocity in the media and the central frequency of the used equipment.

The application of GPR spreads to concrete investigations, characterization of human constructions (modern and historical buildings, archaeology), forensic sciences and geological fields (tectonics, sedimentology, geomorphology, mining, etc.; see Daniels, 2004 or recently Annan, 2009 and references therein for applications). The application of GPR usually has an important handicap related to low penetration depth in high conductivity media. This problem is shared with other EM and electric equipments where high conductivity media can produce the weakening of reflection (GPR), wave refraction and higher wave scattering.

The results obtained by means of GPR represent returning amplitude traces from the subsoil in a qualitative scale, usually ranging from −1 to 1. The GPR results can be plotted in a colour or white and gray scale (radargrams). The lateral correlation of similar changes in the amplitude trends are observed as bands with lateral continuity in the GPR-profiles, permitting the interpretation of geometrical changes between reflectors as layering changes and variations of EM properties. The identification of other features can be done by analyzing the changes in thickness of bands in the GPR-profile

* Corresponding author.
*E-mail address:* opueyo@unizar.es (Ó. Pueyo-Anchuela).

0926-9851/$ – see front matter © 2011 Elsevier B.V. All rights reserved.
doi:10.1016/j.jappgeo.2011.07.002

(apparent qualitative changes of the propagation velocity), reflector definition (reflectivity changes) or lateral variations of attenuation (loss of definition of the reflectors or strong decrease in the penetration depth). These qualitative aspects can give information, under controlled conditions, of clay content, EM properties and changes in the state of the subsoil.

The qualitative analysis of changes in the GPR-wave by means of the amplitude of the energy-decreasing sinusoidal wave has been postulated as an efficient tool for determining the lateral correlation of net changes in the subsoil. The most relevant application field has been the identification of archaeological structures (Conyers, 2004; Conyers and Goodman, 1997; Conyers and Cameron, 2006; Ernenwein, 2006; Forte and Pipan, 2008; Goodman, 1996; Goodman and Nishimura, 1993; Goodman et al., 1995, 1998; Gracia et al., 2007; Grealy, 2006; Leckebusch, 2000; Leucci and Negri, 2006; Pipan et al., 1992; Shaaban and Shaaban, 2001) or location and analysis of graves (Doolittle and Bellantoni, 2010) within others. This semi-quantitative approach is based on the search for strong dielectric changes related to walls, roads, or other anthropogenic materials that usually develop hyperbolic anomalies in GPR-profiles (anomalies related to the sharp dielectric changes). The identification of these changes by means of amplitude analysis can be also aided by changes in propagation velocity and the wave lags at the target and below it (vertical propagation of superficial changes that progress along the whole analyzed sample). These echoes are stronger in metallic elements giving multiple refractions. Radargrams show then the vertical propagation of the same reflector through apparently increasing TWT intervals. This kind of approaches have been used in other cases different to archaeological surveys to laterally correlate lateral net changes in the subsoil related with faults (Demanet et al., 2001; Green et al., 2003), to infer hydrogeological characteristics and permeability models (Asprion and Aigner, 1997; Corbeanu et al., 2002; McMechan et al., 1997; Szerbiak et al., 2001), internal characterization of infrastructures (Sudarmo et al., 1996), establish the drainage pipe patterns (Allred et al., 2008) cartography of clay content or clayish areas (De Benedetto et al., 2011; Weaver, 2006), internal characterization of karst processes (Kruse et al., 2006; Pueyo-Anchuela et al., 2009) or internal characterization of sediments by means isolated triggers (Nielsen et al., 2009), or to correlate sedimentary structures at glacio-fluvial deposits (Beres et al., 1999), gravel deltas (Asprion and Aigner, 2000), fluvial channels (Corbeanu et al., 2001), aeolian river dunes (van Dam, 2002), coastal barriers (Jol et al., 2002) or multidisciplinary analysis for sedimentary structures, fractures and archaeological features (Grasmueck et al., 2004).

Amplitude grid-maps (semi-quantitative approach) are not systematically used for sediments characterization while C-scans are usually employed for chair and cube presentations in many disciplines (e.g. Daniels, 2004 or preceding references). This amplitude lateral correlation is one of the bases of 3D models, but systematic analyses have only been applied up to date in a limited number of publications out of the archaeological studies (see for example Chamberlain et al., 2000 for karst cavity detection or clay content or clayish areas mapping at Weaver, 2006 or De Benedetto et al., 2011).

Recently, semi-quantitative techniques have started to be applied to GPR surveys, by means of the analysis of the wave amplitude, to obtain porosity/permeability ratios, water content, pollution plumes, grain size or to define sedimentological facies through the application of stochastic methods (see for example van der Kruk, 2001 or Moysey et al., 2003). All these fields represent a promising future for semiquantitative GPR interpretation.

In order to analyze the real meaning of lateral correlation of wave-amplitudes, two field tests where GPR-profiles can be directly compared with quarry trenches were done. The objective is to analyze the record of B-scans (profiles or radargrams) and qualitative amplitude changes and their actual meaning through comparison with outcrops. From the obtained conclusions in both sections a subsequent field survey was developed in an area with no exposures, analyzing GPR-profiles through amplitude grid maps, and comparing with an EM broadband multifrequency survey. The studied areas present clear internal sedimentary structure, in some cases linked to synsedimentary karst activity (see Luzón et al., 2008 for analysis of sedimentary deposits architecture linked to karst activity).

## 2. GPR layout and methodology

GPR waves adjust to a symmetrical sinusoidal curve. The amplitude of the reflected wave depends in a first approximation on the reflectivity. The usual way to present GPR data consists of radargrams (B-scans), representing the wave amplitude by a qualitative coloured scale. This kind of plot permits the visual assessment of lateral correlation of similar changes in radargrams related to wave amplitude variations. These changes are related to variations of the type and state of materials and their internal structure (see Neal, 2001 and references therein). This way to analyze GPR data can be aided by qualitative interpretation of: potential higher propagation velocity (using the thickness changes of the horizontal banded disposition of the GPR waves in the subsoil) or apparent changes in attenuation observed through the loss of potential penetration depth (loose of reflector definition). These changes in test grounds or well-known areas can be ascribed to changes in lithology, material characteristics, clay content or state change (see for example Reynolds, 1997; Annan, 2009). This methodology represents the qualitative approach to GPR analysis.

In addition to this more visual way to characterize GPR data, radargrams can be exported to a spreadsheet with a XZI coordinate system (X = horizontal distance or traces; Z = depth at TWT or sample and I wave amplitude according to a decreasing sinusoidal wave with amplitudes ranging from −1 to 1). This sinusoidal pattern is the origin of the banded disposition of radargrams. Analysis of amplitudes for C-scans also uses a fourth coordinate for relative position between profiles (Y). C-scans are developed through the definition of a referring element, correlating element or pixel that is defined by its size with X,Y and Z (dimensions and coordinates). The general definition of pixel size should be higher than (1) triggering interval, (2) horizontal and vertical device resolution, (3) distance between parallel profiles and (4) size of identified elements to be analyzed. In the same way, the same methodology developed for C-scan can be applied to isolated profiles, the obtained data similar to B-scans depend on the same characteristics of pixel size than C-scans (to avoid confusions B-scans where amplitude quantitative analysis was applied will be called Am-scans).

The I value for an isolated trace (trigger) is defined by the amplitude of the sinusoidal wave; when pixel size exceeds one measurement point, I value should be calculated from the statistical meaning of each data. On one hand the representative I value for each pixel can be calculated by developing means, highest or lowest representative values or even as an intensity factor for the whole data sum or maximum change rate. In practice, the definition of pixel size should follow the same expected for C-scans, aided by the Z size higher than the wavelength. In the same way, with independence of the I calculation method (in this work the pixel average has been used) the banded disposition inherent to GPR sinusoidal pattern at amplitude treatment can be avoided by using absolute or squared values in opposite to I raw data. For absolute or squared values, the I value of analyzed pixel, can be used in first approach, as a measurement of apparent reflectivity, independently from the sinusoidal pattern). The presence of wave lags and changes in the propagation velocity can be the responsible for non homogeneous pixels, being in these cases the abnormal values of I indicative of changes in the studied interval. Squared values are the most commonly used because they maximise differences from the mean data distribution. Relative wave amplitude changes (relative reflectivity) can also be used for this kind of analysis by the calculation of the change factor that provides

comparable intervals at different depths with independence of gain filters (see examples of different methodologies in Fig. 1). On the other hand, the definition of pixel size can be used as a stacking process (or running average filter).

## 3. Test of Am-scans at exposures

Three GPR devices with central frequencies of 50 (unshielded), 100 and 250 MHz (shielded; Mala Geoscience) were used for field sampling. The two test-grounds were selected in areas without potential noise sources and horizontal even topography. Triggering distance was established with density higher than the expected horizontal resolution (0.3, 0.1 and 0.01 m) to avoid significant loss of resolution if stacking were needed. The data filtering depended on the objective of the analysis. For the qualitative interpretation based in the direct observation of the GPR-profiles, the filtering is used for profile saturation. The routine included several steps: (i) filtering out of range frequencies for each of the equipments, (ii) application of gain filters to increase the wave signal with depth (applying a first constant increase gain and a second exponential gain) and (iii) stacking where needed (when the horizontal displacement was not regular: usually no more than 3× for the shielded devices and up to 9× for unshielded). No topographic corrections were applied.

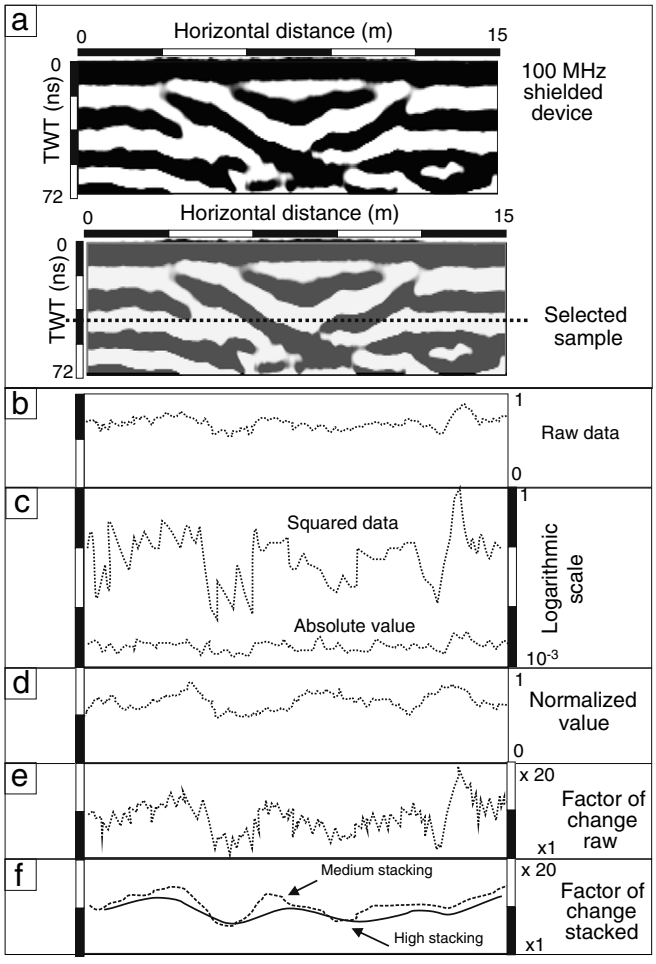


**Fig. 1.** (a) GPR-section where a plane-concave geometry can be observed. The selected sample has been marked in the radargram. Different plots of this selected sample from the profile have been used to test the potential results in (b) raw data, (c) squared and absolute, (d) normalized value, (e) factor of change or relative amplitude for the studied sample and (f) differences of stacking to the factor of change or relative amplitude.

### 3.1. Case 01

In Case 1 the trench (Fig. 2) shows structures related to paleo karstic activity: a collapse in its western edge (laterally delimited by vertical contacts and filling accommodation with on-lap geometries and thickening in its central zone) and a potential paleo-subsidence area in its eastern sector (plane-concave geometry). Between both areas horizontal bedding is affected by minor small subvertical and E-dipping faults. The studied units consist mainly of gravels and sands related to terrace levels with higher clay contents in the fillings of the collapse and subsidence areas.

GPR-profile (100 MHz; Fig. 2b) shows sharp limits, consistent with the collapse walls observed in the outcrop. The western border of the collapse shows a hyperbolic anomaly and at its eastern border the contact between the collapse area and the host rock can be characterized as a steeply dipping reflector, both in the GPR-profile and the exposure. To the east of the collapse area a general horizontal attitude of the sediments can be observed. In the eastern zone of the profiles steeply dipping reflectors are associated with a paleochannel shape, where dips increase to the East, become horizontal, and in the eastern border of the profile dip shallowly in the opposite sense. Below the western limit of this plane-concave geometry, a hyperbolic anomaly appears. These changes in the radargram can be correlated to changes in dip of beds. On the other hand, in the central to eastern zone of the profile, some dip changes can be correlated to small E-dipping faults.

Am-scan was applied to analyze the influence of changes of the I value used and pixel size changes. For I raw value, Am-scan (Fig. 2c) presents a main banded horizontal disposition. Changes in the horizontal banded disposition can be ascribed to slight changes in the propagation velocity generating an apparent out-of-phase displacement and the distortion of the banded horizontal disposition (in homogeneous soils this banded disposition should remain similar along the whole analyzed section). I = factor of change (Fig. 2d) exhibits a decrease of influence of intensity with depth while the banded distribution is still present. Absolute values of factor of change for I at Am-scan (Fig. 2e and f) indicate the disappearance of the banded pattern. The main difference between both figures (Fig. 2e and f) are related to stacking (increase of pixel size). For low stacking (small pixel size; Fig. 2e), relative positive anomalies can be associated with geometrical changes in the radargrams. These anomalies, mainly positive, occur independently from hyperbolic anomalies (cases of the lateral limits of the collapse area or changes in the dip of the reflector in the eastern zone of the profile). Contacts of the collapse area correlate with changes in the amplitude trends and delimit an inner zone between them with lower relative values (negative anomaly) related to a potential lower reflectivity. At the progression to the East, the described plane-concave geometry in the exposure develops at a change in the Am-scan amplitude trend; most part of the eastern zone can be related to a relative positive I value where bedding dip changes are associated with relative negative anomalies.

The positive area in the central-eastern sector (Fig. 2d) does not show corresponding features in the outcrop, although it contains higher I values. When compared with the radargram it can be observed that this zone is related to steeply E-dipping reflectors. From a detailed geometrical analysis subvertical contacts probably related to collapse structures can be seen. For increasing pixel size (Fig. 2f) the influence of isolated anomalies seems to disappear in the Am-scan and the most important features develop according to changes in soil characteristics. The zone related to the sedimentation and accommodation to a subsidence focus and a collapse exhibits a relative negative anomaly contrasting with areas of the profile associated with relative positive values. The subsidence areas show, in both cases, finer grain-size (host rocks: gravel and sands, subsidence areas: sands and clays). Comparison between the correlation of Am-scan (Fig. 2e) and the

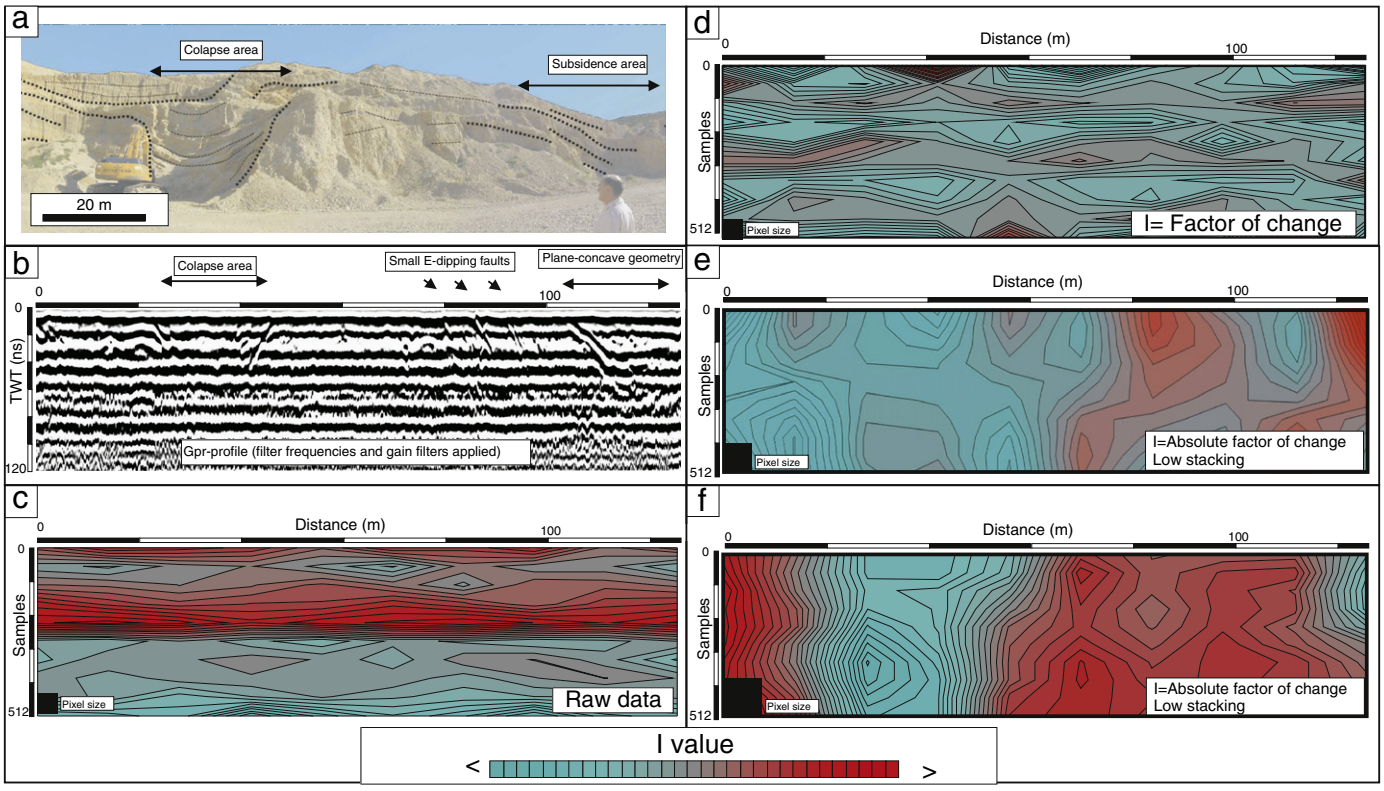


**Fig. 2.** Paleokarst quarry exposure, case study 1. (a) outcrop photograph with line drawing for the interpretation of some features at the exposure, (b) GPR-profile obtained for superficial conditions using the 100 MHz shielded device (only filter frequency out of range and linear gain have been applied for profile saturation). Am-scans for different data processing (c) plotting of Am-scans for I = raw data where horizontal distribution and the skin depth imprint can be observed; (d) Am-scans for I = factor of change; (e and f) Am-scans for I = absolute value for factor of change for (e) intermediate pixel size (low to middle stacking) and (f) large pixel size (high stacking). In the different Am-scans the pixel size for scan has been added for each subfigure (in black, in lower-left corner of each scan).

geometry of the deposits is good whereas the direct correlation with the GPR-profile is not so evident (similar aspects are usually found when high stacking, that corresponds to apparent profile migration, is applied to a GPR-profile).

### 3.2. Case 02

Case 2 test-ground (Fig. 3a) shows gravels with nearly horizontal bedding in the upper part of the series, underlain by horizontal beds abutting against a vertical contact in the western part of the profile and a syncline with progressive onlap geometries from a thickened subsidence center. The eastern border of the collapse-subsidence area does not show an only clear vertical contact, but different steeply dipping contacts and bending of some of the stratigraphic levels out of the collapse area. This geometry evolves, in the eastern part of the section, to a general westward dip of the rest of the series, where cross-bedding can be also observed in the gravel unit located in the eastern zone.

Radargram (cf = 100 MHz, Fig. 3b) shows a strong internal structure. Comparing with the outcrop photograph, a clear parallelism between the general structure of the outcrop and the identified reflectors can be observed. On the other hand, the subvertical contacts observed in the quarry section are not clearly represented in the radargram. In the western limit of the profile a weak hyperbolic anomaly related with the actual fault can be observed while in other zones the sharp change of reflector dips can be used to locate the karstic collapse (fault identified by dipping of reflectors rather than by hyperbolic anomalies or fault parallel reflectors).

Plotting of raw I Am-scan (Fig. 3c) shows a horizontal banded disposition with apparent higher attenuation in the central zone of the profile (apparent lower I values if they are laterally compared). This apparent weakening of the wave amplitude (and I value) in the zone of the subsidence area correlates with higher clay content. Bending of the first positive band appearing in the depressed central zone of the profile can be potentially related to a change of the propagation velocity in the clay-rich filling of the subsident zone.

The contacts that delimit the collapse and subsidence area observed in the quarry are not directly developed at the radargrams. However, representation of I = absolute factor of change (Fig. 3d) indicates very important changes related to these contacts. The subvertical contacts of the collapsed area can be correlated to clear changes in style in the Am-scans, with sharp changes in the trends of I values, thus associating the main part of the collapse area with a relative positive anomaly with respect to the host-rock. According to the outcrop photograph, the western limit of the collapse area is sharp and only several meters wide. The eastern border of the collapse shows subvertical sharp changes, bended reflectors and parallel, steeply W-dipping faults. This more complex limit is not so well-defined in the Am-Scan (Fig. 3d). In the case of the bended and subsident area, I values show a broad negative relative anomaly that nearly correlates with the filling of the central syncline of the collapsed area where higher clay content can be identified at the studied outcrop.

### 3.3. Considerations of Am-scans at quarry exposures

Am-scans of apparent reflectivity obtained in both quarry sections exhibit a general correlation with the identified geological structures. The presented results permit to answer some questions about the application of amplitude grid maps with different equipments, different filtering techniques and the correlation between real structures and features identified in radargrams and Am-scans. About the changes of sedimentary materials there is a higher dependence of internal structural changes

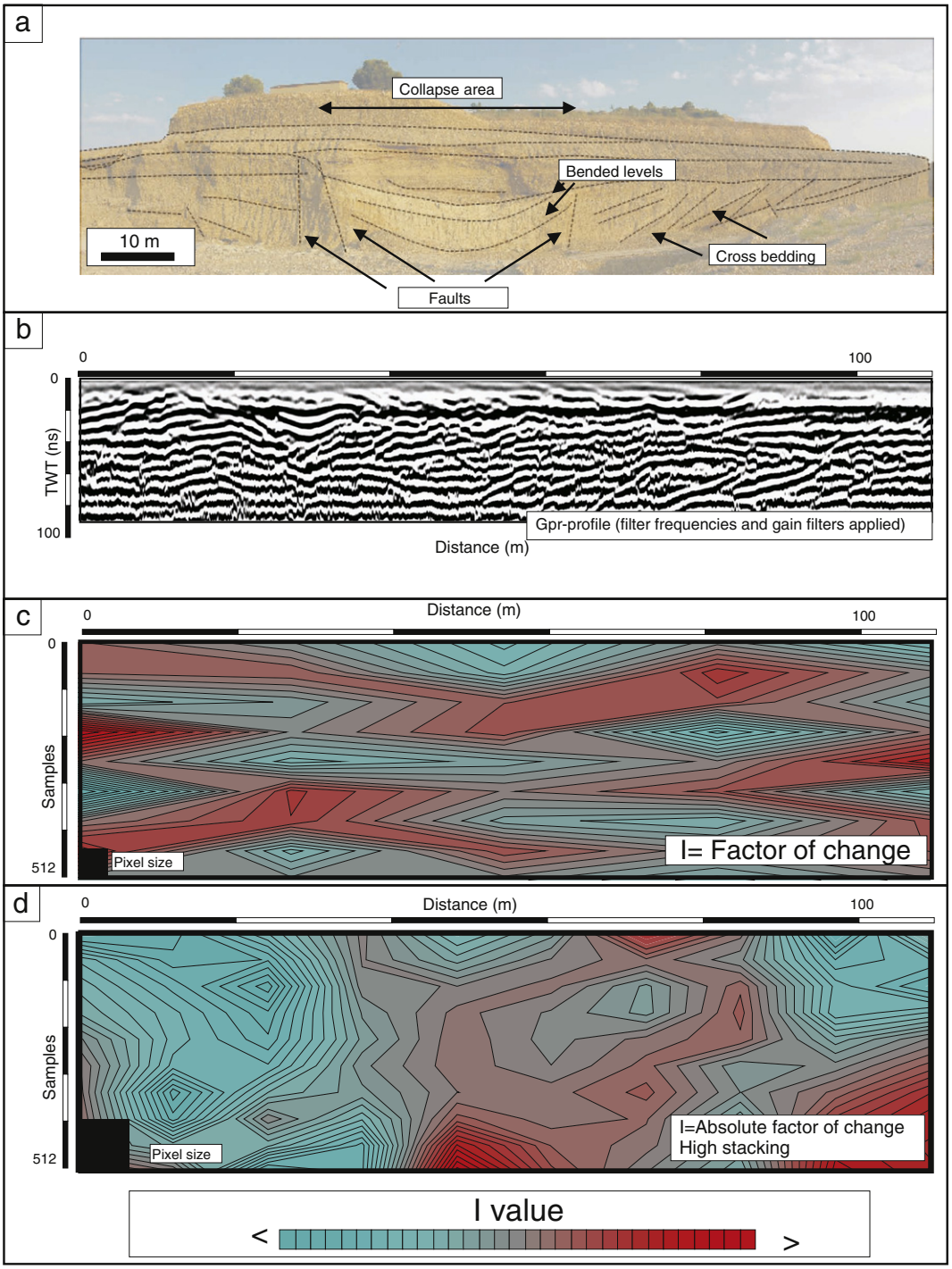


**Fig. 3.** Paleokarst quarry exposure, case study 2. (a) outcrop photograph with line drawing for some of its geological features. (b) GPR-profile obtained for superficial conditions using the 100 MHz shielded device. (c) Am-scan for I = relative factor of change; and (d) Am-scan for I = absolute factor of change for big pixel sizes (high stacking).

for small pixel sizes (usually more controlled by vertical lags and out-of-phase waves) and a higher dependence of changes of soil type for higher pixel sizes.

These geometrical changes between reflectors (case of on-lap or wedge geometries) can be related to changes in the propagation velocity, developing lateral wave lags (as it happens in hyperbolic anomalies without geometrical changes in layering) while in most cases there are layer-parallel changes in radargrams. In the studied ground-tests the comparison between photographs and profiles shows that the reflector slopes are more dependent on the bedding dip than on the change in the potential propagation velocity. In these cases, and because of the pixel size (in the sense of stacking): i) for correlation of small geometrical changes between reflectors, with independence of their association with hyperbolic anomalies, low stacking is recommended and ii) the changes between the host materials and the surveyed element are magnified through high stacking (or larger pixel size). In these conditions, relative positive or negative anomalies from Am-scans serve as a semiquantitative indirect measurement of EM properties (attending to different attenuation or reflectivity).

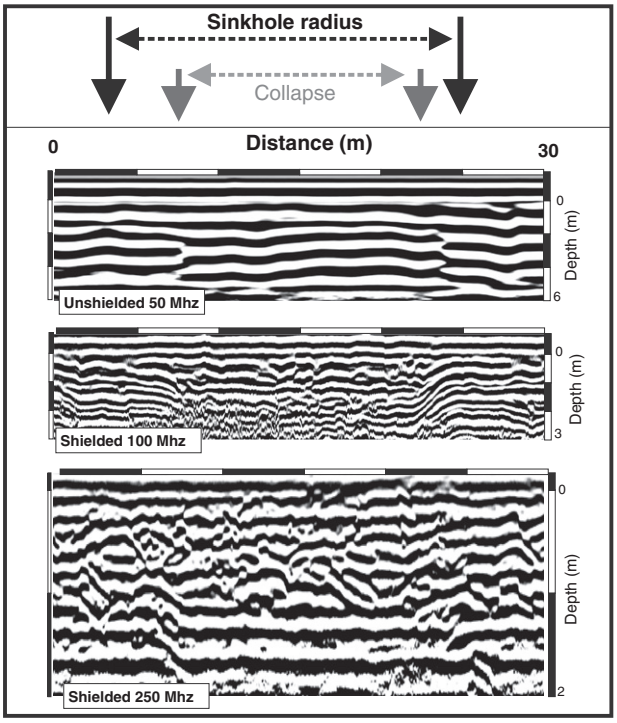


**Fig. 4.** Radargrams (B-scans) obtained for the test-site with three different GPR central frequency antennas (50, 100 and 250 MHz). The processing was applied to saturate the GPR-profiles and to analyze the geometrical changes between reflectors. Superficial radius of karst historical activity have been added for collapse area according to field indicators (open cracks, subvertical superficial terrain faults) and external radius (sinkhole radius) linked to vegetational growth and slight topographical changes affecting the analyzed surface (profiles have been developed avoiding these topography changes around the collapse).

## 4. Application of GPR grid maps to 3D characterization of sedimentary structures

In order to analyze the potential application of described methodology, a survey in a flat area with no exposures was done. The survey grid includes parallel profiles for 50, 100 and 250 MHz. EM broadband multifrequency survey was also done in order to double-check the obtained results. Geomorphological and superficial data indicate a karstic collapse subsequently filled with urban debris to level the surface. The filling materials underwent settlement, thus enforcing several filling episodes. This information is useful to test the presence of a potential record of the settlement and subsidence process.

In first approximation, the used devices have different potential penetration depth and different resolution (Fig. 4). The three profiles over the same sinkhole have been plotted considering only the upper part of the soil (in the usual skin depth zone, where geometrical features and changes are easily observed). Lower stacking, band pass filter and linear gain were applied with the objective of profile saturation. From superficial data two different envelope radii were measured, representing (i) the old collapse that is surrounded by open cracks and filled with urban debris and (ii) an external expected radius inferred from differential vegetation growth or small changes in the topography. In an overall view, the three profiles show similar geometrical signatures, usually onlap geometries with centripetal dips. The limits of the collapse present a sharp change that can be related to hyperbolic anomalies (250 MHz), apparent loss of continuity of reflectors and change in the apparent attenuation (100 MHz) or sharp lateral changes in the banded disposition (50 MHz). The three profiles show geometrical changes between reflectors beyond the collapsed area, extending laterally to the left side of the profiles. The right end is more abrupt and beyond the collapse area they show a homogeneous, parallel horizontal banded disposition.

In the 50 MHz profiles no changes other than the limits of the collapse and the general trend of reflector adaptation from the left side of the profile can be observed. In the case of the other two antennae, a more detailed analysis of geometrical relations and reflectivity changes can be done. In the case of 100 MHz, changes in the reflector disposition in the proximities of the collapse and hyperbolic anomalies and geometrical changes in the filling of the collapse can be observed. Moreover, a change in reflectivity or attenuation can be detected when comparing the results from the collapse and the host sediment, observing an apparent higher attenuation in the inner zone of the collapse area. In the 250 MHz radargrams, the changes in reflectivity and attenuation are not so evident (GPR-profile was nearly saturated to increase the possibility of identifying geometrical changes). However, clear hyperbolic anomalies related to the margins of the collapse, those become subvertical limits in the sides of the collapsed area, can be identified. The filling of the collapse also shows hyperbolic anomalies and inhomogeneous behaviour that indicate the probable existence of other potential subsidence foci within the identified collapse located at the right side of the profiles.

The same methodology applied to isolated profiles (Am-Scans) was used for amplitude grid maps (C-scans). The plotting of the uppermost slice, for each device (Fig. 5a), represents a depth interval between 0 and 1.4 m (0 to 28 ns). The plotted slices have used I absolute relative amplitude for plotting (relative amplitude: the lower amplitude value for each interval was used for relative changes to be calculated). For each plot the colour scale was established from the variation spectrum in each map. In the three cases a maximum can be observed in the collapse area. The strongest changes can be observed in the case of 50 MHz, with a zone with a maximum rate of change of 450× in the northern part of the collapse. In the cases of 100 MHz and 250 MHz the maximum strength does not indicate the collapse area, developing one maximum in its southern zone (100 MHz) or two different maxima (250 MHz) instead. However, the envelope of these anomalies follows the collapse area and the internal envelope of the 50 MHz survey. The rate of change of I value decreases by a factor of 320× in the case of 100 MHz and 42× in the case of 250 MHz. When grid maps are compared with the radargrams (Fig. 5), higher amplitude values appear at the filling of the collapse in the 50 MHz. In the cases of 100 and 250 MHz shielded devices, the strongest changes detected from grid maps occur in areas with thicker filling or higher reflectivity (or stronger inhomogeneous behaviour) and in areas corresponding to geometrical changes in the radargrams, developing in both cases relative maxima over the southern limit of the collapsed area (that can be related to a sharp change of the wave behaviour, and hyperbolae in the southern border of the collapse in both profiles). In the northern sector an adaptation of reflectors can be seen with the 100 MHz and a hyperbola with the 250 MHz antenna, with a better definition of the contact in the 250 MHz device.

The analysis of different depth slices shows, in the case of unshielded equipment, a progressive influence from the superficial anomaly along the vertical section, developing a vertical propagation of the high reflectivity zone identified in the central zone of the profile (related to the filling of the collapse). In the case of shielded devices the echoes related to the shallower anomalies (change in the attenuation of the filling or high reflectivity elements) do not control the maps at higher depths. Both 100 and 250 MHz results are similar at depth. In the case of 100 MHz (Fig. 5b) the shallower maps shows a direct influence of the collapse area but, this influence disappears below 4 m.

The I relative factor values vary for the different used devices and with the analyzed depth. The general decrease with the penetration depth can be expected if no gain is applied, by the decrease of the wave energy with depth and with the increase of the first Fresnel zone radius and decrease of the discrimination resolution (homogenization of the wave with depth).

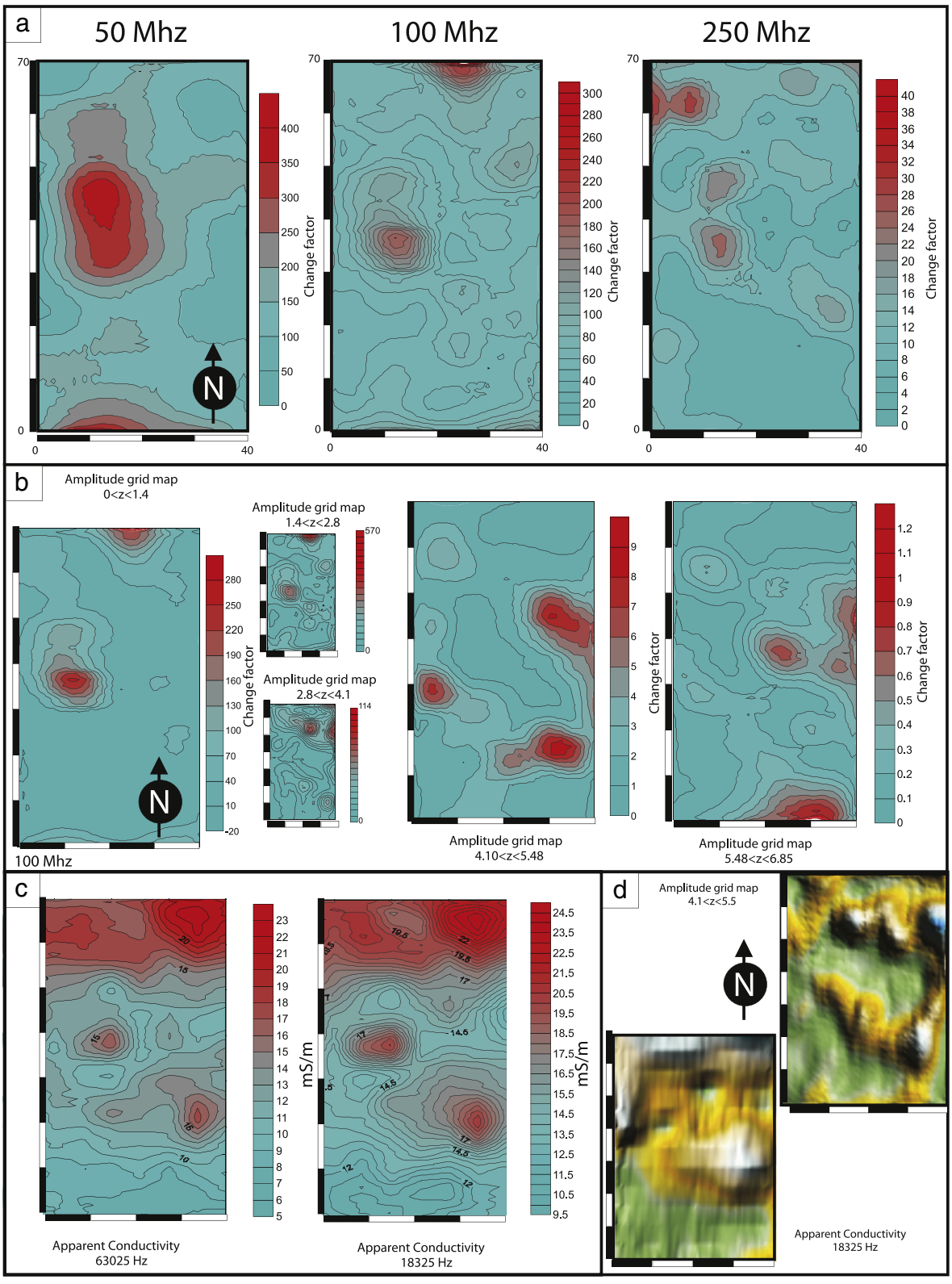


**Fig. 5.** Main results obtained in the test site, (a) amplitude grid maps for the first TWT interval for the 50, 100 and 250 MHz devices. (b) TWT amplitude grid maps obtained with the 100 MHz device for progressively deeper intervals (I = absolute factor of change), (c) apparent conductivity obtained with the multifrequency broadband EM radiation device for 63 and 18 KHz frequencies, (d) shaded relief plots for apparent conductivity obtained from EM survey using a frequency of 18 kHz and amplitude grid maps obtained from GPR with the 100 MHz antenna (intermediate depth).

Apart from the anomalies linked to the known collapse area an elliptical disposition of relative maxima in the amplitude grid maps is observed without evidences of collapse at surface. For this reason a multifrequency EM device (Gem-2) was used to perform a double check approach to characterize these identified changes. The EM Gem-02 survey also depends of the electromagnetic properties of the surveyed materials. EM surveys and its modulated wave allow for the apparent susceptibility and conductivity to be calculated through changes in the

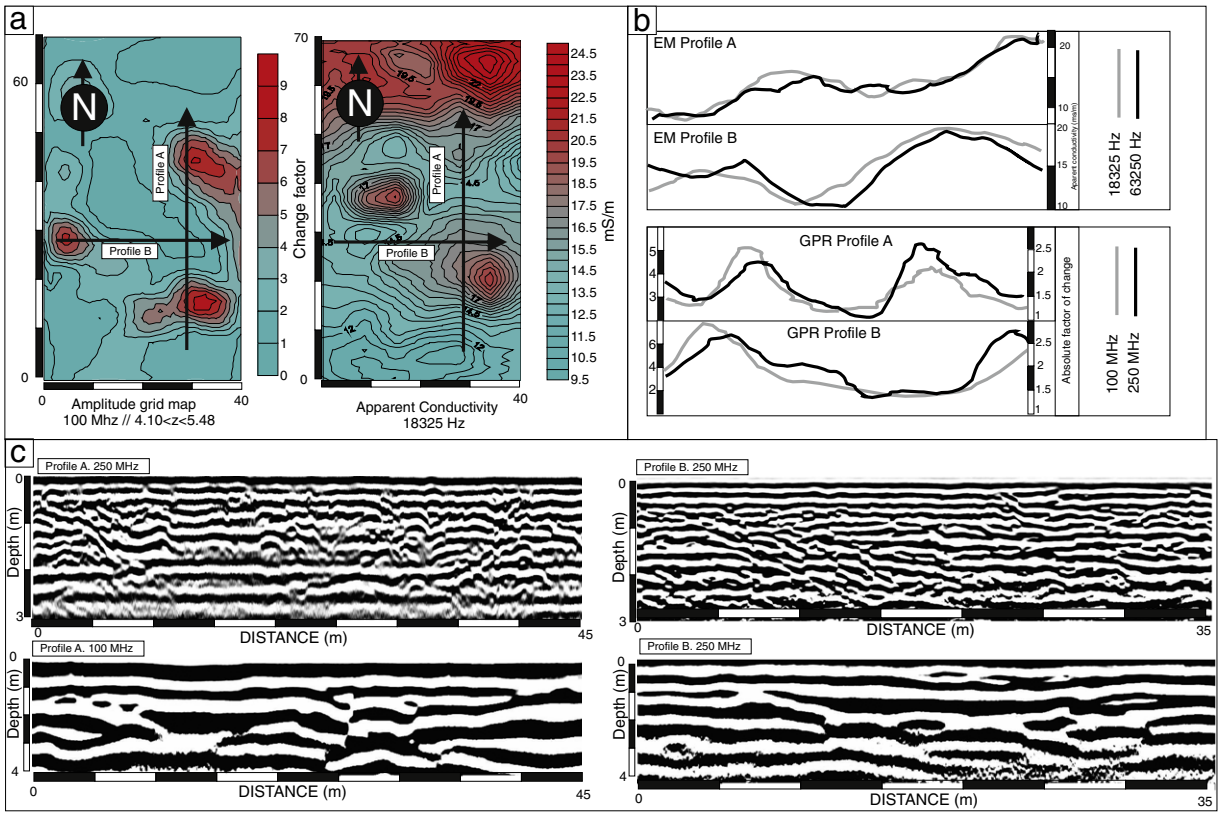


**Fig. 6.** (a) Plots for the apparent conductivity (in mS/m) obtained from EM survey using a frequency of 18 kHz and amplitude grid maps obtained from GPR with the 100 MHz antenna (intermediate depth) in contours for the amplitude grid maps (I = factor of change). The locations of profiles shown in 6.b and 6.c are indicated. (b) Plots of apparent conductivity for 65 and 18 KHz along profiles A and B at (a) and plots of the factor of change obtained with the 100 and 250 MHz devices for the two sections indicated in (a. (c) Radargrams obtained with the 100 and 250 MHz antennae for A and B profiles indicated in (a).

phase and quadrature waves (Huang and Won, 2000). The EM survey was designed according to profiles parallel to the GPR-profiles. Gem-2 device can operate at different frequencies at the same time, permitting the analysis of different depth intervals during survey (Huang, 2005) equivalent to depth slices in GPR grid maps). Apparent conductivity for the higher measured frequencies (63,025 and 18,325 Hz) show an important change in conductivity (5 mS/m for 63,025 Hz and 10 mS/m for 18,325 Hz) in the northern zone. These changes are mainly controlled by shallow elements (the northern limit of the test field is also the boundary of the farming field with a small scarp). Another anomaly with similar values of apparent conductivity can be observed in the central eastern zone, apparently not related to superficial elements.

The comparison of EM surveys and grid-GPR slices shows an inverse relationship, highest values of apparent conductivity coinciding with the lowest values of I. This situation can be more easily observed in the false relief plots (Fig. 5d) where relative positives slice maps surround relative maxima of apparent conductivity. In order to directly compare radargrams, GPR amplitude plots, apparent conductivity maps and sections, two different plots were selected (Fig. 6). I values from GPR slices and the apparent conductivity obtained from the EM survey indicate a zone with an elliptical geometry, with the collapse located in its NW margin, and adaptation features between reflectors that correlate with relative positives in the GPR slices. These relative positives bound a zone with higher apparent conductivity. This anomalous zone identified by EM and grid maps correlates with adaptation features between reflectors with general dip or wedge opening towards the centre of the profiles. In the case of 250 MHZ device a general concave upwards geometry marginally limited by clear dipping reflectors that apparently does not involve the surface can be observed. Similar results were obtained with the 100 MHz device (Fig. 6c and d).

## 5. Discussion. What can really be obtained from grid maps?

The objective of this work is to test the significance and reliability of amplitude grid maps in the characterization of the internal structure of the subsoil. In the studied case, in general terms, the analysis of Am-scans double-checked with quarry exposures permits to interpret the correlation between grid maps and the geometrical changes between reflectors, hyperbolic anomalies and changes in the EM propagation characteristics. The application to a survey area indicates a direct correlation between geometrical changes at GPR-profiles, interpreted geological structures and results obtained from the grid maps and apparent conductivity. The presented results permit to answer some questions about the application of amplitude grid maps with different equipments, different filtering techniques and the correlation between real structures and features identified from GPR surveys (radargrams, Am and C-scans).

From the obtained data, we conclude that the application of amplitude grid maps depends on three factors: the potential influence of changes near the surface, changes of the EM properties of materials and the geometrical changes between reflectors.

Changes in near surface conditions can produce a change in the wave phase in the vertical of the survey; higher propagation velocity, for example, can produce a wave lag that progresses downwards or changes in the attenuation of the waves can contribute to decrease the wave amplitude below the attenuation zone. These changes produce an important wave phase displacement resulting in Am-scans and grid maps anomalies controlled by superficial changes (echoes or residual anomalies), The results obtained in the case of Am-scans indicate that superficial changes do not necessary produce the whole amplitude dependence below them. This aspect permits the application of the described methodology for internal structural characterization (or EM

characteristics) even in cases with strong changes in near surface conditions.

Since Am-scans are dependent of EM properties of the subsoil, propagation velocity and/or dielectric constant, changes in these parameters are mapped by means of time-slices of GPR. In this case, hyperbolic anomalies are strongly dependent on the triggering and the central frequency of the device (potential horizontal and vertical resolution). Some changes are responsible for hyperbolic anomalies in the 250 MHz device, but only produce changes in the reflectors disposition (geometrical relation changes between reflectors) in the 100 MHz device, and just vertical lateral contacts in the reflectors continuity in the 50 MHz device. In the case of the test site, the geometrical changes between reflectors control the amplitude grid maps, rather than the presence of hyperbolic anomalies.

In the case of 250 MHz survey, hyperbolic anomalies do not define a relative maximum at grid maps, and the positive peaks are probably related to changes between reflectors. This is also related to the used pixel size, because isolated anomalies without lateral correlation between profiles nearly disappear in the grid maps. In this way, these changes can represent slight increases in the wave amplitude values of the zone where they are present, while the geometrical changes between reflectors can give place to higher intensity anomalies with lateral correlation.

Filtering of data before the application of amplitude grid maps can generate relevant changes in the map finally obtained. The gain functions can produce the displacing of the wave range to a maximum losing its original symmetry with respect 0. Then, frequency filters are needed to recover the original distribution of the wave pattern. The possibility of identifying geometrical changes in the profiles can then be higher, but after wave processing there is a homogenization and therefore other qualitative indicators (attenuation or reflectivity changes) cannot be used. When low gain is applied, attenuation changes can be better identified if profiles are not saturated. An example of saturation can be observed in Fig. 6b, where in an overall view the I relative value along progressively deeper grid maps decreases. This is true for all the depth intervals except between the first and second (the shallower). In the first interval there is an influence of the direct wave that sometimes is not correctly erased and the wave is almost saturated in intensity. The I factor of change then decreases in the second analyzed TWT interval, while in the rest of the cases an attenuation of the change factor with increasing depth occurs.

This decrease in the factor of change represents also a decrease of discrimination resolution (increase of the radius of the first Fresnel zone or increase of the footprint surface), developing a natural averaging (or stacking) at higher distances than expected in shallower conditions. The identification of changes at different depths can be done by defining slices at different depths. This application can be successful only in cases where ghosts from shallow features are not present. In cases where ghosts or echoes from superficial elements vertically progress in depth, amplitude grid maps can be developed at no real penetration conditions as residual maps (that are in many cases successfully applied to archaeological surveys with time-slice amplitude grid maps as residual or lag-maps).

In the presented case, apparent variations in the attenuation and wave propagation velocity related to changes in clay content of the materials or in urban debris filling do not seem to affect successive, deeper intervals. In the case of 50 MHz antenna, or in high reflectivity elements as iron scrap, echoes are expected to control the real data with independence of the analyzed depth interval.

## 6. Conclusions

The application of semiquantitative characterization of the internal subsoil structure by means of lateral correlation of the wave amplitude of GPR has been analyzed through: (1) comparison between quarry exposures, radargrams and Am-scans and (2) comparison of three different GPR-antennae where radargrams and amplitude time (depth)-slices have been double-checked with an EM multifrequency survey. The results obtained permit to compare changes in radargrams that respond to geometrical layering changes at outcrops and their imprint at Am-scans. There is a good correlation between changes observed in quarry trenches and in the wave amplitude in Am-scans. Lower stacking treatment (small pixel sizes) permits the identification of relative positives in hyperbolic anomalies or changes in the geometrical disposition of reflectors. This correlation permits to establish the potential application of amplitude grid-maps for 3D cartography of geometrical changes (for example sedimentary structures) where high stacking (higher pixel sizes) is useful to indirectly test the semiquantitative EM characteristics of the subsoil materials (by the use of the I relative factor as indirect measurement of the attenuation or reflectivity).

The results obtained in the test site show:

1) The ways to identify and correlate geometrical changes observed in the profiles and related to subsidence and collapse in superficial conditions in amplitude grid maps. Relative positives coincide with geometrical changes (onlap geometries and hyperbolic anomalies).
2) The influence of high reflectivity elements in surficial conditions. In the cases of unshielded devices, superficial elements control the maps of depth slices. In shielded devices, the stronger anomalies correspond to shallow elements, and deeper elements can be observed in progressively deepening time slices, without apparent influence of the most superficial anomalies.

The influence of different features in the grid maps is related to the geometrical changes identified in the profiles. In the case of the comparison between EM multifrequency survey and GPR grid maps, the collapse area is related to a higher apparent conductivity and a positive relative peak of I value for surficial time slices. The external radius related to a zone with higher apparent conductivity is surrounded by adaptation features that give relative positive values.

The results presented permit to identify the applicability of amplitude grid maps at correlating internal structural changes (sedimentary structures) and a semiquantitative approach for EM changes. The use of amplitude grid maps to solve lateral correlation of geometrical features (even in sectors with strong internal structure and lithological changes) represents a methodology worth to be systematically applied as a first approximation to the data and giving a more quantitative interpretation of apparent attenuation or reflectivity, that can be dependent of the filtering routine applied to the profiles. On the other hand, the semiquantitative approach can permit the identification, in a very fast way, of zones of changing behaviours where detailed analysis by qualitative methodologies can be focused. The inverse correlation between apparent conductivity and amplitude grid maps also supports a dependence of both EM techniques and depth-slicing approach on (i) the presence of clay rich materials, (ii) higher apparent conductivity and (iii) parallel decrease of wave amplitude (or higher attenuation factor) that is identified in GPR slices or Am-scans by negative relative anomalies parallel to the apparent conductivity increase.

## Acknowledgements

This work is part of the communication presented in the SG3 conference held in Zaragoza in June, 2009. The authors want to thank the funding from Project DGA PI031/08, the Geotransfer Research Group from Zaragoza University and a pre-doctoral grant to the first author (FPU program). Authors want to thank you the revision, suggestions and recommendations by two anonymous reviewers that have significantly improved the manuscript.

## References


Allred, B.K., McCoy, E.L., Redman, D., 2008. 28- Ground Penetrating radar investigation of a Golf Course Green, Computes Processing and Field Survey Setup Considerations. In: Allred, B.J., Daniel, J.J., Reza Ehsani, M. (Eds.), Handbook of Agricultural geophysics. CRC Press, pp. 353–362.

Annan, A.P., 2009. Electromagnetic Principles of Ground Penetrating Radar. In: Jol, H.M. (Ed.), Ground Penetrating Radar Theory and Applications. Elsevier, Amsterdam, pp. 1–40.

Asprion, U., Aigner, T., 1997. Aquifer architecture analysis using ground-penetrating radar: Triassic and Quaternary examples (S. Germany). Environmental Geology 31, 66–75.

Asprion, U., Aigner, T., 2000. An initial attempt to map carbonate buildups using ground-penetrating radar: an example from Upper Jurassic SW-Germany. Facies 42, 245–252.

Beres, M., Huggenberger, P., Green, A.G., Hortsmeyer, H., 1999. Using two and three dimensional georradar methods to characterize glaciofluvial architecture. Sedimentary Geology 129, 1–24.

Chamberlain, A.T., Sellers, W., Proctor, C., Coard, R., 2000. Cave detection in limestones using ground penetrating radar. Journal of Archaeological Science 27, 957–964.

Conyers, L., 2004. Ground penetrating radar for archaeology. Alta Mira Press, Walnut Creek, CA.

Conyers, L.B., Cameron, C.M., 2006. Ground penetrating radar techniques and three-dimensional mapping in the American Southwest. Journal of Field Archaeology 25 (4), 417–430.

Conyers, L., Goodman, D., 1997. Ground Penetrating Radar: An Introduction For Archaeologist. Altamira Press, Walnut Creek, CA.

Corbeanu, R.M., Soegaard, K., Szerbiak, R.B., Thurmond, J.B., McMechan, G.A., Wang, D., Snelgrove, S., Forster, C.B., Menitove, A., 2001. Detailed internal architecture of fluvial channel sandstone determined from outcrop, cores and 3-D ground-penetrating radar: Example from the middle Cretaceous Ferron sandstone, east-central Utah. American Association of Petroleum Geologists Bulletin 85, 1583–1608.

Corbeanu, R.M., McMechan, G.A., Szerbiak, R.B., Soegaard, K., 2002. Prediction of 3-D fluid permeability and mudstone distributions from ground-penetrating radar (GPR) attributes: Example from the Cretaceous Ferron member, east-central Utah. Geophysics 67, 1495–1504.

Daniels, D.J., 2004. Ground penetrating radar2nd Edition. : IEE Radar, Sonar and Navigation series 15The institution of electrical engineers- Herts, United Kingdom. 719 pp.

De Benedetto, D., Castrignano, A., Sollitto, D., Modugno, F., Buttafuoco, G., G. lo, Papa, 2011. Integrating Geophysical and geostatistical techniques to map the spatial variation of clay. Geoderma doi:10.1016/j.geoderma.2011.05.005.

Demanet, D.L., Evers, G., Teerlynck, H., Dost, B., Jongmans, D., 2001. Geophysical investigation across the Peel boundary fault (The Netherlands) for a paleoseismological study. Netherlands Journal of Geosciences 80, 119–127.

Doolittle, J.A., Bellantoni, N.F., 2010. The search for graves with ground penetrating radr in Connecticut. Journal of Archaeological Science 37 (5), 941–949.

Ernenwein, E.G., 2006. Imaging in the ground-penetrating radar near field zone: a case study from New Mexico, Usa. Archaeological Prospection 13, 155–158.

Forte, E., Pipan, M., 2008. integrated seismic tomography and ground-penetrating radar (GPR) for high resolution study of burial mounds (tumuli). Journal of Archaeological Science 35 (9), 2614–2623.

Goodman, D., 1996. Comparison of GPR time slices and archaeological excavations. proceedings of the sixth international conference on ground penetrating radar, Sendai, Japan 2. Department of Geoscience and Technology, Tohuku University, Sendai, Japan, pp. 77–78.

Goodman, D., Nishimura, Y., 1993. A ground radar view of Japanese burial mounds. Antiquity 67, 349–364.

Goodman, D., Nishimura, Y., Rogers, J.D., 1995. GPR times-slices in Archaeological Prospection. Archaeological Prospection 2, 85–89.

Goodman, D., Nishimura, Y., Hongo, H., Maasaki, O., 1998. GPR amplitude rendering in archaeology. Proceeding of the Seventh International Conference on Ground-Penetrating Radar. University of Kansas, Lawrence, Kansas, USA, pp. 91–92. Radar Systems and Remote Sensing Laboratory, University of Kansas.

Gracia, F.G., Blanco, M.R., Abad, I.R., Sala, R.M., Ausina, I.T., Marco, J.B., Conesa, J.L.M., 2007. GPR technique as a tool for cultural heritage restoration: San Miguel de los Reyes Hieronymite Monastery, 16th century (Valencia España). Journal of Cultural Heritage 8, 87–92.

Grasmueck, M., Weger, R., Horstmeyer, H., 2004. Three-dimensional ground-penetrating radar imaging of sedimentary structures, fractures, and archaeological features at submeter resolution. Geology 32, 933–936.

Grealy, M., 2006. Resolution of ground penetrating radar reflections at differing frequencies. Archaeological Prospection 13 (2), 142–146.

Green, A., Gross, R., Holliger, K., Horstmeyer, H., Baldwin, J., 2003. Results of 3-D georadar surveying and trenching the San Andreas Fault near its northern landward limit. Tectonophysics 368, 7–23.

Huang, H., 2005. Depth of investigation for small broadband electromagnetic sensors. Geophysics 70 (6), G135–G142.

Huang, H., Won, I.J., 2000. Conductivity and susceptibility mapping using broadband electromagnetic sensors. Journal of Environmental and Engineering Geophysics 5 (4), 31–41.

Jol, H.M., Lawton, D.C., Smith, D.G., 2002. Ground penetrating radar: 2-D and 3-D subsurface imaging of a coastal barrier spit, Long Beach, WA, USA. Geomorphology 53, 165–181.

Kruse, S., Grasmueck, M., Weiss, M., Viggiano, D., 2006. Sinkhole structure imaging in covered karst terrain. Geophysical Research Letters 33, L16405.

Leckebusch, J., 2000. Two and three- dimensional ground-penetrating radar to map subsurface archaeological features in an urban area. Journal of Archaeological Science 33, 502–512.

Leucci, G., Negri, S., 2006. Use of ground-penetrating radar to map subsurface archaeological features in an urban area. Journal of Archaeological Science 33, 502–512.

Luzón, A., Pérez, A., Soriano, M.A., Pocoví, A., 2008. Sedimentary record of Pleistocene paleodoline evolution in the Ebro basin (NE Spain). Sedimentary Geology 205 (1–2), 1–13.

McMechan, G.A., Gaynor, G.C., Szerbiak, R.B., 1997. Use of ground-penetrating radar for 3-D sedimentological characterization of clastic reservoir analogs. Geophysics 62, 786–796.

Moysey, S., Caers, J., Knight, R., Allen-King, R.M., 2003. Stochastic estimation of facies using ground penetrating radar data. Stochastic Environmental Research and Risk Assessment 17 (5), 306–318.

Neal, A., 2001. Ground-penetrating radar and its use in sedimentology: principles, problems and progress. Earth-Science Reviews 66 (3–4), 261–330.

Nielsen, L., Moller, I., Nielsen, L.H., Johannessen, P.N., Pejrup, M., Andersen, T.J., Korshoj, J.S., 2009. Integrating ground penetrating radar and borehole data from a Wadden Sea barrier island. Journal of Applied Geophysics 68, 47–56.

Pipan, M., Baradello, L., Forte, E., Prizzon, A., Finetti, I., 1992. 2D and 3D data processing and interpretation of multifold ground-penetrating radar data: a case study from an archaeological site. Journal of Applied Geophysics 41, 271–292.

Pueyo-Anchuela, Ó., Pocoví-Juan, A., Soriano, A.M., Casas-Sainz, A.M., 2009. Characterization of karst hazards from the perspective of the doline triangle using GPR — Examples from Central Ebro Basin (Spain). Engineering Geology 108 (3–4), 225–236.

Reynolds, J.M., 1997. An introduction to applied and environmental geophysics. John Wiley & Sons, p. 806.

Shaaban, F.F., Shaaban, F.A., 2001. Use of two-dimensional electric resistivity and ground penetrating radar for archaeological prospecting at the ancient capital of Egypt. African Earth Sciences 33, 661–670.

Sudarmo, B., McMechan, G.A., Epili, D., 1996. Simulation and imaging of GPR data scattered by reinforcing bars in concrete bridge deck. Journal of Environmental and Engineering Geophysics 1, 163–170.

Szerbiak, R.B., McMechan, G.A., Corbeanu, R., Forster, C., Snelgrove, S.H., 2001. 3-D characterization of a clastic reservoir analog: from 3-D GPR data to a 3-D fluid permeability model. Geophysics 66, 1026–1037.

van Dam, R.L., 2002. Internal structure and development of an aeolian river dune in The Netherlands, using 3-D interpretation of ground-penetrating radar data. Netherlands Journal of Geosciences 81, 27–37.

van der Kruk, J., 2001. Three dimensional imaging of multi-component ground penetrating radar. Ph.D. Thesis, Delft University of Technology. Pp 242.

Weaver, W., 2006. Ground-penetrating radar mapping in clay: success from South Carolina, USA. Archaeological Prospection 13, 147–150.